Journal of Mining and Environment (JME), Vol. 12, No. 2, 2021, 569-587

Shahrood University of Technology

Iranian Society of Mining Engineering (IRSME)

Journal of Mining and Environment (JME)

journal homepage: www.jme.shahroodut.ac.ir

THOMSON REUTERS

Investigation of Geochemical Correlation Between Radioactive and Rare Earth Elements: Case Study of Baghak Mine, NE Iran

Seyyed Saeed Ghannadpour*and Ardeshir Hezarkhani

Faculty of Mining and Metallurgical Engineering, Amirkabir University of Technology, Tehran, Iran

Article Info

Received 4 May 2021
Received in Revised form 29 May 2021
Accepted 3 June 2021
Published online 3 June 2021

DOI: 10.22044/jme.2021.10793.2045

Keywords

Radiation measurement
Radioactivity
Rare earth elements
Baghak
Sangan iron mine

Abstract

In several uranium (U) prospecting projects in Iran, particularly Central Iran, the association and enrichment of rare earth elements (REEs) are known as the usual features. Sometimes the association of REEs and U with high economic perspective has caused that the relation between the rare earth and radioactive elements is taken into consideration in other types of mineralization, and if there is any relation, radioactivity will be applied in the exploration of REEs. In the current work, sampling from Baghak anomaly in the Sangan mines is carried out based on the radioactivity and radiation measurement methods (as the optimal sampling pattern). In fact, the goal of this work is to survey the presence or absence of such a relation in a skarn mine, which is a different case study from Central Iran. In the case of presence, this will lead to a new exploration method and sampling pattern for REEs. The mineralogical studies (based on the optical and electronic microscopic observations), statistical investigations, and geochemical analyses are applied in this research work. The results obtained from the statistical studies show that the Baghak anomaly due to involving a significant amount of U, Ce, and La and a high concentration of REEs can be considered as one of the important mines. Spider diagrams and their geochemical investigations include the features that are typical of the subduction-related magmas in the calcalkaline volcanic arcs of the continental active margins. The chondrite-normalized REE pattern shows the enrichment of LREE, and a positive pattern close to flat HREE due to the entry of LREE ions into the allanites network. The mineralogical study results also confirm that REEs (especially Ce) are accumulated as a solid solution in the allanite minerals. Moreover, from the mineralogical, geochemical, and statistical analyses, it can be observed that in addition to the presence of such a relation in the mentioned mineralization (Central Iran mineralizations), there is an acceptable correlation between these elements in the Baghak iron-skarn mineralization. Eventually, it can be said that the idea and introduced method for the exploration of REEs in this work could present a new viewpoint to the decision-makers of this industry.

1. Introduction

It is noteworthy that in several prospecting projects of uranium (U) that belong to the Atomic Energy Organization of Iran (AEOI), and particularly Central Iran zone, the association and enrichment of Rare Earth Elements (REEs) are recognized as a common feature. Sometimes, the association of these elements with U by the values greater than the economic limit has caused that genetic modelling of U-REE, exploration geochemistry analysis, and mineral processing studies of these elements in the semi-industrial phase taken into consideration in parallel processes [1].

This association and enrichment of the REEs is commonly seen in the metasomatite type. It has also been observed in a skarn type mineralization in Central Iran.

Corresponding author: s.ghannadpour@aut.ac.ir (A. Hezarkhani).

Many studies have shown evidences of the presence of REEs in the Sangan iron ore mine, which is known as the biggest skarn iron ore deposit in western Asia [2]. The Sangan iron ore mine is located at a distance 300 km SE of Mashhad in the Khorasan-e Razavi Province, NE of Iran. Some of these studies are summarized below.

Boomeri has studied REEs in the Sangan iron mine, in which the concentration of REEs in garnets measured by LA-ICP-MS in Akita University of Japan has been reported [3-4]. In other studies by Mazhari et al. [5-7] in the Sangan and eastern anomalies of Ferezneh and Senjedak-I, the ratio of LREE/HREE in Ferezneh has been reported from 58.2 to 78.13. Also the moderate enrichment of LREE and positive anomaly of Eu in geochemical data have been observed in this anomaly [5]. In Senjedak-I, the REE values show the Eu negative anomaly, moderate enrichment of LREE, positive pattern close to flat HREE, and finally, negative anomaly of Ba, Sr, La, Ce, Ti, and Eu [6]. In the study of Golmohammadi et al. in some eastern anomalies, it can be seen that the spider diagram normalized with the average continental crust show enrichment in HFSE, Zr, Nb, Ga, Ta, Y, and Hf and depletion in Ba and Sr, and these features belong to the post-orogenic granitoids [8]. They also showed that in some western and central anomalies, the relative enrichment of LREE proportion to HREE in normalized pattern to chondrite and enrichment of LILE proportion to HFSE elements in normalized pattern to primary mantle in intrusive bodies show the formation of magma in the subduction zone [2, 9-10]. Gholipour et al. have analyzed the geochemical data in order to determine the nature and origin of the REE mineralization fluids, the physico-chemical conditions of REE concentration, and the pattern of REE distributions in this zone. The collected samples of skarn-ore and host rocks show the LREE enrichment relative to HREE in the iron ore and skarn zones [11].

Moreover, Sepidar et al. have investigated the mineral geochemistry of the Sangan skarn deposit in order to achieve implication for the evolution of the hydrothermal fluid. The last above-mentioned study show that in the Sangan skarns, hydrothermal fluids have shifted from near-neutral pH, reduced conditions with relatively high REE, low LREE/HREE ratios, and U-rich characteristics towards acidic, oxidized conditions with relatively low REE, high LREE/HREE ratios, and U-poor characteristics [12].

Investigation of the rare earth and radioactive elements has been carried out in other research works in Iran and elsewhere in the world, which, for example, could be cited to the studies of relation of alkali-metasomatism and Ti-REE-U (Th) mineralization in the Saghand (Central Iran) by Deymar et al. [13], and investigation of the relationship between rare earth elements, trace elements, and major oxides in soil geochemistry by Vural [14], spatial variability and geochemistry of REEs in soils from the largest uranium–phosphate deposit (Brazil) by Cunha et al. [15], REE/trace element characteristics of sandstone-type uranium deposits in the Ordos Basin (China) by Ling et al. [16], etc.

Therefore, in this work, according to the evidence of their existence (REEs) in the Sangan mine and the observed relation in many studies carried out by AEOI (about metasomatite and skarn type), the exploration of REEs is initially done using the radioactivity and radiation measurement methods in Baghak anomaly, which is located in the Sangan iron mines. Then normalized REE distribution patterns (based on the chondrite and primitive mantle) are investigated, and finally, the normalized REEs distribution pattern of the Baghak mine is compared with the REE distribution pattern related to several different types of iron deposits (skarn, Banded Iron Formation (BIF), hydrothermal and Kiruna).

2. Studied area

The Sangan iron ore deposit is 300 km far from SE of Mashhad, 68 km from SW of Tibad, 40 km from SE of Khaf, and 18 km from SE of Sangan in the Khorasan-e Razavi Province, and they are located near the border of Iran-Afghanistan [8, 17]. The area is shaped as a rectangular 22 km long and 10 km wide, which includes the western deposits (A, A', B, northern and southern C), central deposits (Baghak and Dardvey), and eastern deposits (Figure 1) [10]. Another view of the western and central anomalies is available in Figure 2, which shows the seven deposits of A, A', B, northern C, southern C, Baghak, and Dardvey along with major faults. The Baghak anomaly is the target area in this work, which is located in the central part of the Sangan mine. The Baghak ore deposit is in eastern border of C and 250 m south of the Dardvey deposit. The longitude of this anomaly is from 266400 to 268300 E, and its latitude is from 3817200 to 3818700 N, which involves an area of 285 ha. 239 boreholes have been drilled from the beginning of the prospecting

procedure in this ore deposit by a total length of 62997 m. The mentioned boreholes include core samples, and finally, 6641 analyses have been carried out [18].

The Sangan iron ore deposit is part of the volcanic-plutonic belt of Khaf-Kashmar-Bardeskan. If we consider the continuation of the magmatic belt of Khaf-Darouneh to Afghanistan from one side and to Biarjmand from the other side, it is more than 350 km long, and has a varying width of 15 to 80 km. This belt mostly comprises acidic to intermediate volcanic rocks and somewhere mafic rocks by the age of Tertiary. These rocks include dacite, rhyodacite, andesite, pyroxene-andesite, andesite-basalt, latite, trachy-andesite, tuff, lapilli-tuff, and agglomerate. The granitoid bodies comprising granite, granodiorite, diorite, and alkali granite-feldspar have intruded into the volcanic rocks [8, 17]. The geological map and Fe bodies in the Sangan mine from west to east including A, A', B, northern and southern C, Baghak, and Dardvey are shown in Figure 3 [10].

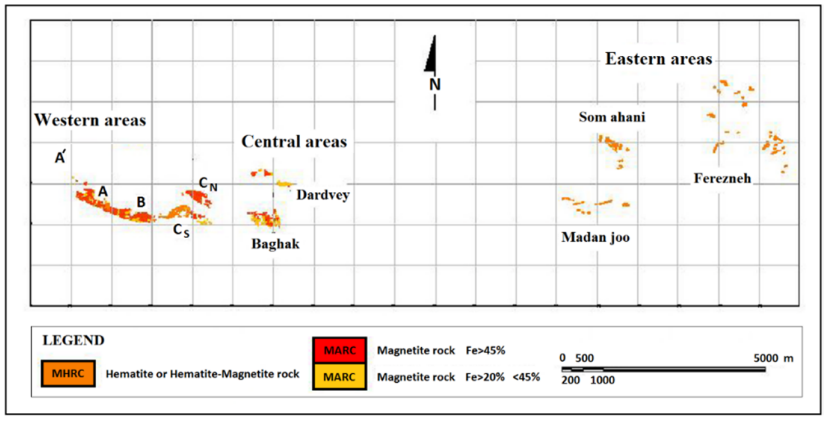

Figure 1. Position of western and central anomalies in the Sangan deposit.

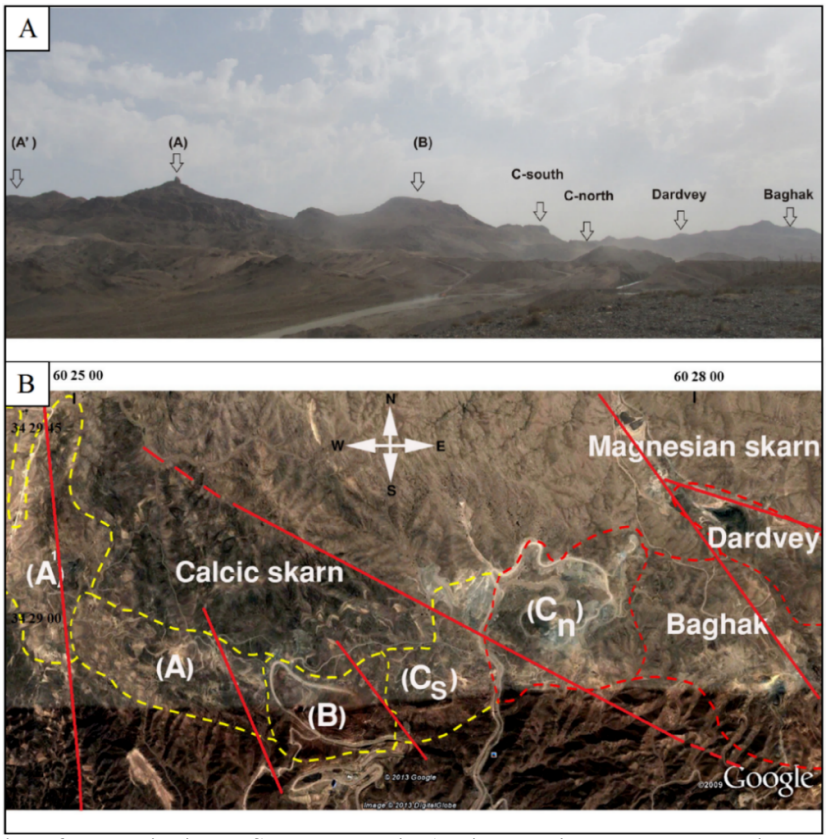

Figure 2. Position of anomalies in the Sangan deposit. A: view looking north, B: top view showing faults of district [10].

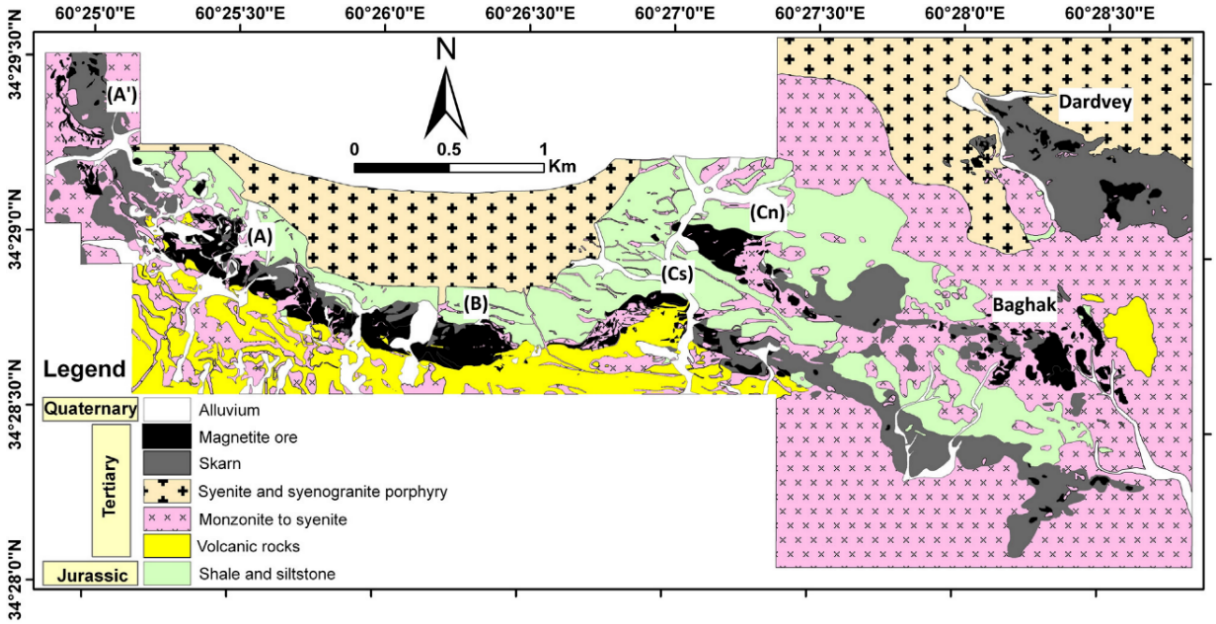

Figure 3. Simplified geological map of the Sangan deposit along with location of magnetite masses in the western and central anomalies [10].

The oldest formations in the studied area include chert, silicified shales, siltstone, and crystallized limestone. Several outcrops from them can be observed in the northern part of ore bodies striking E-W. Enormous volcanic rocks that are mostly related to the volcanic activities of Cretaceous to the early Eocene are obvious in the studied area. The volcanic rocks include dacite, rhyodacite, trachyte, and andesite volcanoclastic. The carbonate rocks are mostly metamorphosed to the skarn and marble, and crystalized limestone has appeared to the east [2].

In the northern part of the mine, Sarnosar granite by the probable age of upper Eocene-lower Oligocene has intruded. Boomeri has introduced the Sarnosar granite as the origin of skarn [3] but Karimpoor and Malekzadeh [17] have delineated that K-enriched minerals such as particular amphibole in the A' body or K-bearing minerals like phlogopite in Baghak and C bodies imply that an Fe-bearing magmatic solution that is also enriched with K has intruded into the carbonates by the metasomatism replacement, and this process has led to the formation of skarn magnetite that is enriched with K-bearing minerals [17].

3. Materials and methods

The sampling operation in the current work was carried out from the drilling cores according to the viewpoint of the relation between REEs and the radioactive elements. The potential radioactive spaces and significant P-bearing cores (based on the geochemical analysis of drilling cores) are the base of sampling. According to this fact, sampling is divided into two parts:

Part I: Applying logs from some boreholes.

It is noteworthy that logging was carried out in only 24 boreholes of the Baghak anomaly, and direct radiometry seems essential for the detailed surveying of the relation between radioactivity and REEs.

Part II: Direct spectrometry operation of drilled cores and selecting radioactive samples using portable hand-held spectrometer, RS 230, manufactured by Radiation Solutions Inc., Canada.

First, the maximum CPS using logs from each borehole was specified, and high values were determined for sampling (Figure 4). Then the boreholes that should be more investigated were determined along with the length of maximum radioactivity. That way, the boreholes by the radioactivity less than 1000 CPS are in the second priority for hand radiometry, and the boreholes by the higher radioactivity than 1000 CPS are applied in the first priority for validating the logging results, obtaining primary information from the studied area and starting the sampling operation.

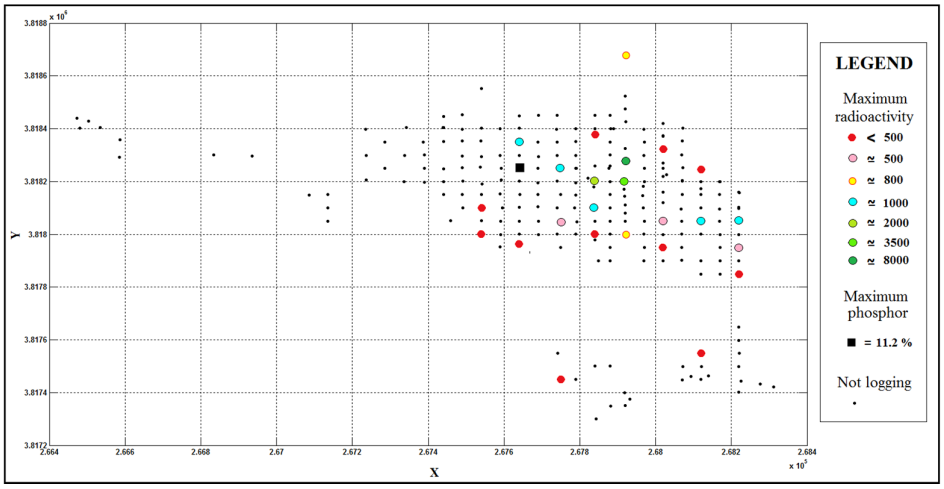

Figure 4. Map of maximum radioactivity of boreholes on their collars.

Then in the first step of sampling in the core-sample warehouse, the determined boreholes were referred, and spectrometry was carried out in the considered length or maybe throughout the boreholes. After preliminary surveying of the drilled cores, the primary information including the background and desired radioactivity of the studied area were determined; the mentioned values are presented in Table 1.

Table 1. Basic information about the studied area.

Background radioactivity (CPS)	Radioactivity in core library (CPS)	Optimal radioactivity threshold (CPS)
200-250	250-300	800

In the next step, according to the information obtained, the regular and detailed radiometry and sampling were carried out. First, logged boreholes by the radioactivity higher than 1000 CPS were investigated, and then the non-logged boreholes were considered, and the samples were taken from the points by the higher relative radioactivity. It is noteworthy that the samples were not taken from the points, and totally, 151 samples in different intervals from unit length (by the centre of maximum radioactivity) were taken (from 10 cm to 3 m).

Then for a detailed study of the relation between REEs and the radioactive elements, the samples were ordered based on radioactivity (measured by a spectrometer), and the first 47 samples along with 3 samples from borehole BK25 including high P concentration were selected for the microscopic studies. Figure 5 shows the boreholes of 47 mentioned samples (radioactivity of greater than 950 CPS).

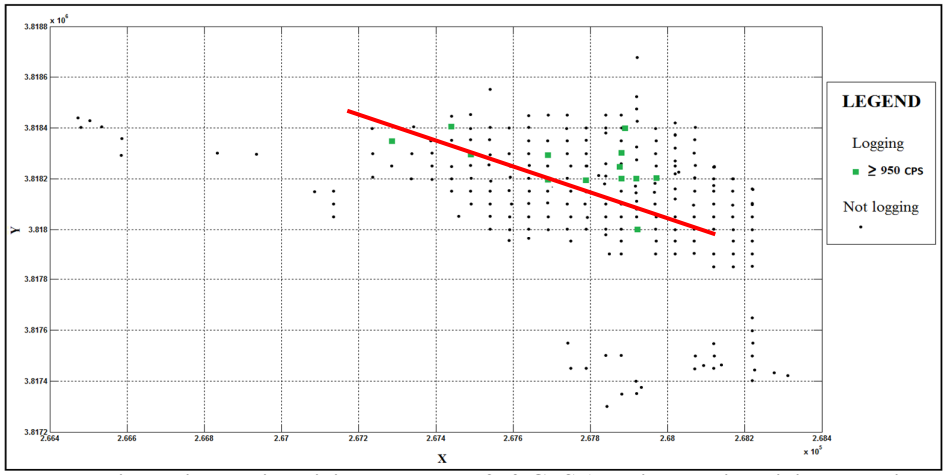

Figure 5. Boreholes including radioactivity more than 950 CPS (red line: radioactivity trend in the region).

Figure 5 shows the radioactive boreholes and general radioactivity in the Baghak anomaly striking NW-SE. As a matter of fact, the radioactivity trend of the studied area follows the faulting strike in the Sangan mine, which particularly coincides with the fault located in the northern C anomaly (Figure 2). This fact increases the probability of radioactive element-bearing mineralization along the faults located in the studied area.

Then the radioactivity of the samples was considered as the base of selecting them for providing thin sections and microscopic studies (using optical microscope (Leitz German make) and electronic microscope (SEM XL30, Philips, Netherlands)). For this purpose, the rock including the maximum radioactivity in each sample bag was selected using a scintillometer (SPP2 manufactured by SAPHYMO, France) for providing thin and polished sections. Before providing the sections, the samples were studied macroscopically; the results obtained are available in Table 2.

3.1. Specimen preparation for analysis

After providing and studying the sections, the residuals of the considered rocks were returned to the bag of each sample, and 151 samples were packed and sent to the Zarazma laboratory (Tehran, Iran) for the ICP-MS analysis. (In addition, 15 duplicate samples were selected in order to check the precision and 2 PRMs (secondary reference materials) in order to check the accuracy.) The ICP-MS analysis by different detection limits for various elements was carried out for each sample, and the concentrations of 56 elements for each case were reported. The elements along with their detection limits are presented in Table 3. In the following, preparing the samples and then their primary statistical analyses for investigating the correspondence between REEs and radioactive elements are discussed computationally.

Table 2. Mineralogy and radioactivity of selected samples for preparation of the sections (thin and polished).

Sample ID	CPS	Section type		Mineralogy
		Thin	Polish	
94-EXP-SN-01-01	350	*	*	Magnetite-Pyrite-Amphibole?
94-EXP-SN-08-02	100	*	*	Pyrite-Amphibole?
94-EXP-SN-09-03	80-100	*	*	Magnetite-Pyrite
94-EXP-SN-10-04	100	*	*	Carbonate
94-EXP-SN-11-05	250	-	*	Magnetite-Amphibole?
94-EXP-SN-14-06	300	*	*	Calcite-Pyrite-Amphibole-Pyroxene-Magnetite
94-EXP-SN-15-07	250-300	*	*	Phlogopite-Biotite-Pyrite-Feldspar
94-EXP-SN-17-08	250-300	*	*	Pyrrhotite? -Amphibole?
94-EXP-SN-22-09	250-300	*	*	Magnetite-Pyrite-Feldspar-Amphibole?
94-EXP-SN-24-10	300	*	*	Pyrite -Silica -Biotite
94-EXP-SN-25-11	300	*	*	Pyrite-Amphibole-Pyroxene
94-EXP-SN-30-12	200-230	-	*	Pyrite-Magnetite-Carbonate
94-EXP-SN-31-13	220	*	-	Magnetite
94-EXP-SN-32-14	200	*	*	Carbonate-Chloride-Amphibole
94-EXP-SN-33-15	150	*	*	Magnetite-Pyrite-Amphibole-Pyroxene
94-EXP-SN-34-16	300	*	*	Pyrite-Magnetite-Calcite
94-EXP-SN-36-17	320	*	-	Magnetite-Pyrite
94-EXP-SN-37-18	150	*	*	Amphibole-Chloride-Magnetite
94-EXP-SN-40-19	300	*	*	Magnetite-Pyrite
94-EXP-SN-43-20	1000	*	*	Magnetite-Pyrite-Amphibole minerals?
94-EXP-SN-45-21	400	*	*	Magnetite-Pyrite-Amphibole minerals?
94-EXP-SN-46-22	300	*	-	Magnetite-Amphibole minerals?
94-EXP-SN-49-23	200	*	*	Carbonate-Silica-Phlogopite
94-EXP-SN-50-24	200	*	*	Phlogopite-Biotite-Carbonate-Pyrite
94-EXP-SN-22-25	250-300	*	*	Carbonate-Amphibole
94-EXP-SN-25-26	300	-	*	Pyrite-Carbonate-Amphibole minerals
94-EXP-SN-17-27	250-300	*	-	Pyrite-Carbonate-Silica
94-EXP-SN-17-28	250-300	*	-	Phlogopite-Biotite-Amphibole-Pyrite
94-EXP-SN-15-29	250-300	*	-	Phlogopite-Biotite-Carbonate
94-EXP-SN-50-30	250	*	-	Phlogopite-Magnetite-Amphibole

Table 3. Analyzed elements using ICP-MS along with detection limits for them.

Element	Cu	Cs	Cr	Co	Ce	Cd	Bi	Be	Ba	As	Al	Ag
DL	1	0.5	1	1	0.5	0.1	0.1	0.2	1	0.1	100	0.1
Unit	ppm	ppm	ppm	ppm	ppm	ppm	ppm	Ppm	ppm	ppm	ppm	ppm
Element	Mo	Mn	Mg	Lu	Li	La	In	Hf	Gd	Fe	Eu	Er
DL	0.1	5	100	0.1	1	1	0.5	0.5	0.05	100	0.1	0.05
Unit	ppm	ppm	ppm	ppm	ppm	ppm	ppm	ppm	ppm	ppm	ppm	ppm
Element	Sn	Sm	Se	Sc	Sb	S	Pr	Pb	P	Ni	Nd	Nb
DL	0.1	0.02	0.5	0.5	0.5	50	0.05	1	10	1	0.5	1
Unit	ppm	ppm	ppm	ppm	ppm	ppm	ppm	ppm	ppm	ppm	ppm	ppm
Element	Zn	Yb	Y	W	V	U	Tl	Ti	Th	Te	Tb	Ta
DL	1	0.05	0.5	1	1	0.1	0.1	10	0.1	0.1	0.1	0.1
Unit	ppm	ppm	ppm	ppm	ppm	ppm	ppm	ppm	ppm	ppm	ppm	ppm
Element	Ca	Dy	K	Na	Rb	Sr	Tm	Zr				
DL	100	0.02	100	100	1	1	0.1	5				
Unit	ppm	ppm	ppm	ppm	ppm	ppm	ppm	ppm				

It is noteworthy that all the preparations were done in the Zarazma laboratory. Actually, the whole of the collected rock samples were grinded by a jaw crusher to the size of 1 mm, and afterward 200 g of that result was comminuted to -200 mesh; it was also necessary to be wary about any pollution of samples while they were prepared.

4. Results

4.1. Optical and electronic microscopic studies

From the samples selected in the previous section, 24 polished sections and 27 thin sections were provided; the section type for each sample is available in Table 2. However, according to the significant similarity of the samples and results, and also the limitation of page number, the results are presented briefly in this section. Based on the comprehensive studies of the thin and polished sections, no evidence is available for the presence of REEs such as monazite, bastnaesite, apatite, and xenotime (e.g. Figures. 6 and 7). It was revealed that identifying the radioactive element-bearing minerals like uraninite was not possible by an optical microscope. However, it should be noted that a significant amount of sphene and allanite as a network of fine to coarse minerals was studied in most of the sections (Figures. 6 and 7).

According to the high amount of sphene and allanite observed in the section petrography, the probability of existing REEs in them was considered as one of the important presumptions. Allanite is from the epidote group, and the general formula is $Ca_2(Al,Fe)_3(OH)(SiO_4)_3$ [19]. Fe, Ce, and Al entered the solid solution of the mentioned composition under particular conditions, and allanite was generated by the formula $(Ca,Fe^{2+})_2(Al,Ce,Fe^{3+})_2(OH)(SiO_4)_3$ [20-22]. Thus it is probable that allanite involves REEs like Ce in the studied area, and then the SEM studies were considered. Finally, a detailed study of the sections by SEM was carried out in the Amirkabir University of Technology (AUT) SEM laboratory.

Figures resulting from studying the thin sections of 94-EXP-SN-43-20 and -01-01 are Figures. 8 and 9. In Figure 8 C, after U scanning by a microscope, it was revealed that the light spot in Figure 8 A corresponded to the U-bearing mineral, and the mineral around it corresponded to Fe (magnetite) (Figure 8 B). As it can be observed, U is not in the form of a solid solution in the REE-bearing minerals.

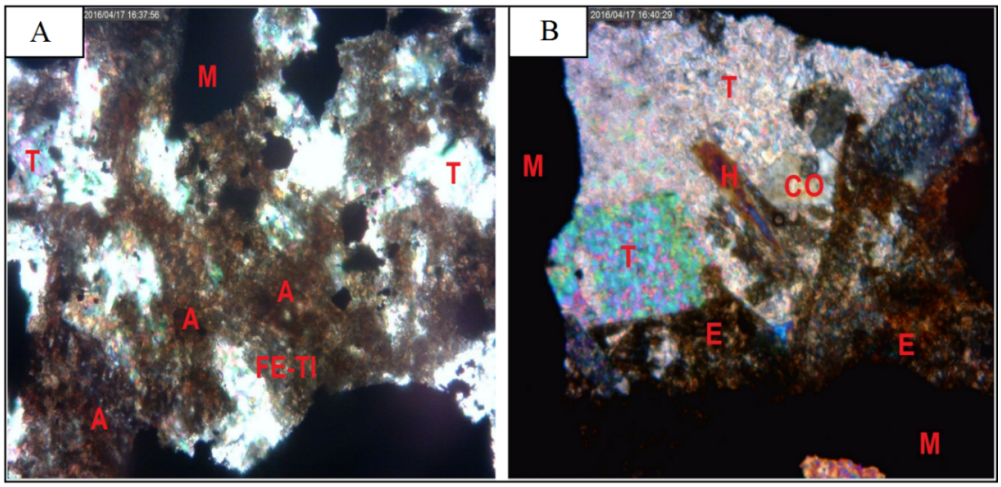

Figure 6. Images of thin section 94-EXP-SN-11-05. A: Displaying small minerals of allanite in keeping with amorphous Fe–Ti oxide and talc beside the magnetite. B: Coarse talc together with fine-grained of the ones resulting from carbonate-silicate are seed at different temperatures. The amorphous epidote minerals apparently formed from the silicatization of Fe–Ti oxides in the presence of carbonate along with magnetite. Amphibole as a type of hastingsite was also seen individually (H = amphibole, M = magnetite, T = talc, E = epidote, A = allanite, FE-TI = Fe–Ti oxide, Co = cordierite).

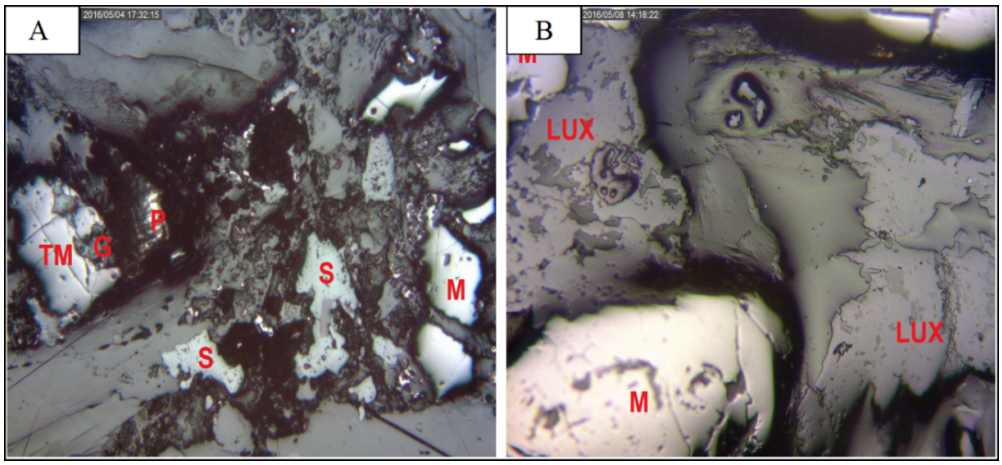

Figure 7. Images of polished sections. A: 94-EXP-SN-15-07, the accumulation of small and amorphous magnetite minerals and the presence of pyrite with strong corrosion texture along with titanium magnetite (goethitization of titanium magnetite). Amorphous sphene is seen along with gangue and magnetite. B: 94-EXP-SN-33-15, single magnetite mineral and accumulation of leucoxene around it could indicate the presence of allanite (G = gangue, M = magnetite, TM = titanium magnetite, S = sphene, LUX = leucoxene, P = pyrite).

According to Figure 8, due to the more specific gravity of U compared to the other elements like Fe, U is lighter than the others. This is true in the case of Fe and other elements, and also other minerals.

Then it was determined that the REEs and most of all cerium accumulated in the allanite minerals (Figure 9).

According to the scans carried out for Ca, Al, Si, and Ce, the dark and light grey colored mineral in Figure 9 A is delineated as allanite, and the increase in Ce as solid solution in allanite cause the darkness.

4.2. Geochemical analysis of samples

For analysing the results obtained, investigating the presence or absence of any relation between REEs and radioactivity or radioactive elements, the data resulting from the geochemical analysis was processed. First, the statistical pre-processing was carried out on the geochemical data, and after determining the primary statistical characteristics (univariate statistical analysis), the presence or absence of correspondence was considered between radioactivity and REEs using the multivariate statistical studies.

Initially, the incorrect cases (possible additional characters, outliers or any typos in the data that cause problems in computations) were corrected in the data files. Then the censored data was replaced by appropriate values (according to the lower detection

limit reported in Table 3). If the censored data involved a low number of total (less than 15%), they would be replaced by 0.75 and 1.25 of the device detection limit (below limit and above limit, respectively); otherwise, due to the inappropriate effects of these elements on the results of the statistical analysis, the foresaid elements were removed. There is a complete report on removing and replacing the censored data in Table 4.

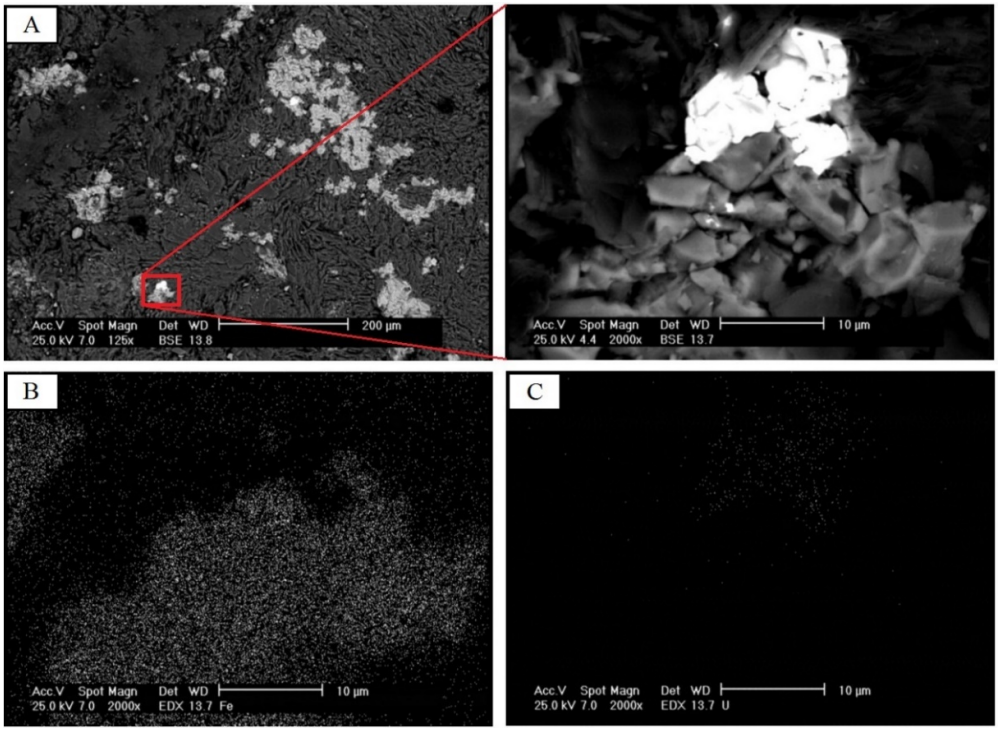

Figure 8. A: Displaying minerals containing uranium and iron in thin section 94-EXP-SN-01-01, B: Scan result for U, C: Scan result for Fe.

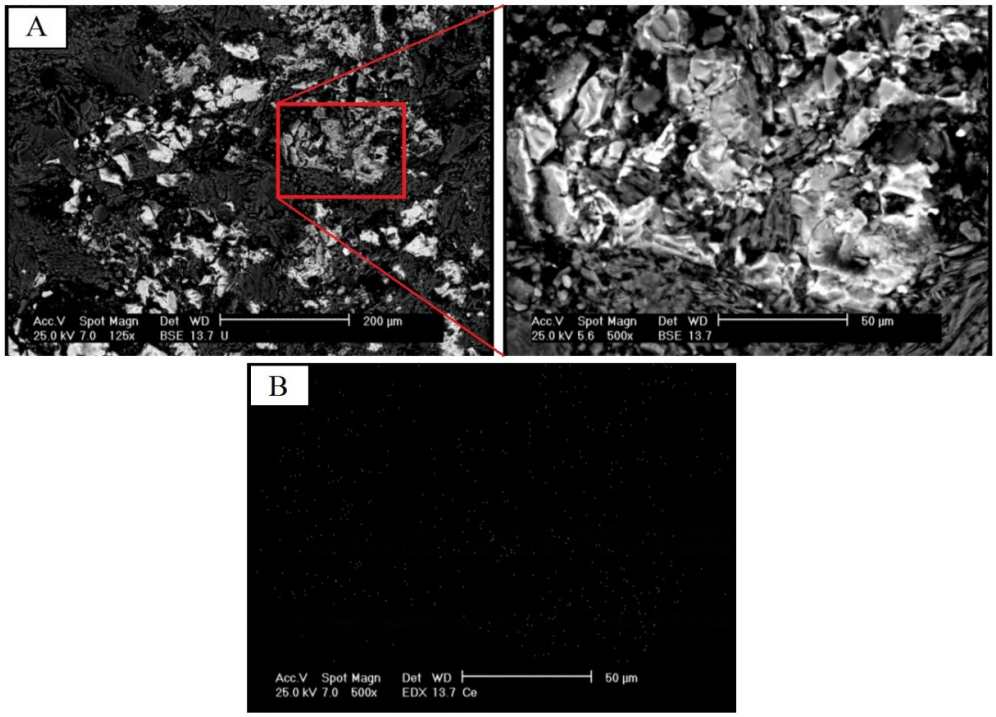

Figure 9. A: Displaying allanite in thin section 94-EXP-SN-43-20 along with magnification of it. B: Scan result for Ce.

Table 4. Characteristics of the censored data about radioactive and REEs along with several main and trace elements in the Baghak anomaly of Sangan.

Element (ppm)	DL	Type of DL	Number of censored data	Percent of censored data	Replacement condition	Replacement value
U	0.1	Below	0	0	-	-
Th	0.1	Below	0	0	-	-
K	100	Below	1	0.66	Yes	75
Fe	100000	Above	123	81.46	No	-
Sc	0.5	Below	41	27.15	No	-
Y	0.5	Below	0	0	-	-
La	1	Below	0	0	-	-
Ce	0.5	Below	0	0	-	-
Pr	0.05	Below	5	3.31	Yes	0.0375
Nd	0.5	Below	0	0	-	-
Sm	0.02	Below	3	1.97	Yes	0.015
Eu	0.1	Below	7	4.64	Yes	0.075
Gd	0.05	Below	0	0	-	-
Tb	0.1	Below	7	4.64	Yes	0.075
Dy	0.02	Below	0	0	-	-
Er	0.05	Below	0	0	-	-
Tm	0.1	Below	5	3.31	Yes	0.075
Yb	0.05	Below	6	3.97	Yes	0.0375
Lu	0.1	Below	14	9.27	Yes	0.075
P	10	Below	0	0	-	-
Ca	100	Above	6	4	Yes	130000
Mn	5	Below	0	0	-	-
Ti	10	Below	0	0	-	-
Al	100	Below	0	0	-	-
Cu	1	Below	2	1.32	Yes	0.75
Pb	1	Below	0	0	-	-
Zn	1	Below	0	0	-	-
S	30000	Above	17	11.26	Yes	40000

As it could be seen in Table 4, the two elements Sc and Fe were removed from the statistical analysis due to involving more than 15% of the censored data. The other elements were studied. Then the anomalous values were investigated as the outliers. However, due to prevention of losing worth anomalous values (according to the sensitivity of losing anomalous values as outliers), it was avoided to remove the outliers since the determined outliers did not seem unreasonable, and they could be considered as high grade values [23].

It is noteworthy that all the calculations for pre-processing (in this section) and statistical analysis (in the next sections) were performed by the MATLAB software (the sub-routines and main programs were coded by the authors).

4.2.1. Univariate analysis

After correcting and preparing the geochemical data, the weighted average of grade for 151 investigating samples (without ignoring non-mineralized samples taken for investigating the relation between REEs and radioactivity) and also mineralized samples (83% of samples) were calculated and presented in Table 5.

It is noteworthy that 26 samples out of the 151 samples collected in this work (approximately 17%) belong to low radiation zones (10 samples without radioactivity and 16 samples with a low radioactivity).

As it could be seen in the above table, the amount of REEs in the total samples decreased compared to the mineralized samples. In this work, the REE concentrations were strongly dependent on the amount of radioactivity, especially the uranium concentration. The REE grade changes in proportion to the uranium concentration and radioactivity so that in the non-radioactive samples, a sudden decrease can be observed in the grade of REEs.

4.2.2. Multivariate analysis

The correlation coefficients for the considered variables (i.e. grade of REEs, U, Th, and K, and also radioactivity) were calculated for a detailed study of their relation. The Spearman correlation coefficient was applied on the investigated variables (non-transformed data) in the Baghak area, and the results obtained were tabulated in Table 6. In addition to this table, the dispersion diagrams of the main parameters (CPS, REEs, U, Th, and K) are illustrated in Figure 10.

Table 5. Primary statistical characteristics of radioactive and REEs along with several main and trace elements in the Baghak district.

Element	Average grade of total samples (ppm)	Average grade of mineralized samples (ppm)	Maximum grade (ppm)
U	185.62	259.84	923.8
Th	25.93	33.36	138.42
K	14454.14	15841	50284
Y	35.34	43.92	145.7
La	958.76	1276.68	6308
Ce	1125.86	1512.03	6566
Pr	99.91	135.95	605.87
Nd	262.48	365.23	1394.2
Sm	23.36	31.43	126
Eu	4.39	5.87	29.16
Gd	18.75	25.09	91.16
Tb	2.16	2.85	12.37
Dy	8.82	11.38	40.96
Er	4.27	5.35	18.15
Tm	0.53	0.65	2
Yb	3.28	4.22	16.7
Lu	0.44	0.56	1.9
∑ REE	2548.37	3412.2	15312.23
P	299.75	315.10	1144
Ca	34156.91	35593.94	96866
Mn	771.29	716.38	2344
Ti	904.91	934.08	3192
Al	21940.83	22975.07	66934
Cu	169.26	127.36	847
Pb	12.20	10.88	92
Zn	102.55	101.75	303
S	17675.55	14000.69	29715

Table 6. Spearman's correlation coefficients for REEs and radioactive elements along with several main and trace elements.

	Spearman's correlation coefficients												
	U	**Th**	**K**	**CPS**	**P**	**Ca**	**Mn**	**Ti**	**Al**	**Cu**	**Pb**	**Zn**	**S**
U	1	0.63	0.45	0.91	0.11	0.17	0.15	0.21	0.49	-0.42	-0.14	-0.09	-0.37
Th	0.63	1	0.52	0.52	0.23	0.12	0.18	0.38	0.61	-0.56	-0.21	-0.04	-0.43
K	0.45	0.52	1	0.46	0.43	0.24	0.51	0.58	0.9	-0.52	-0.26	-0.43	-0.52
CPS	0.91	0.52	0.46	1	0.15	0.24	0.18	0.28	0.47	-0.36	-0.07	-0.18	-0.35
Y	0.70	0.83	0.50	0.59	0.23	0.32	-0.03	0.49	0.6	-0.39	-0.11	-0.09	-0.33
La	0.71	0.83	0.45	0.61	0.21	0.20	-0.02	0.30	0.53	-0.44	-0.18	-0.02	-0.35
Ce	0.72	0.86	0.46	0.61	0.20	0.18	-0.04	0.31	0.55	-0.48	-0.20	-0.02	-0.38
Pr	0.71	0.88	0.46	0.59	0.22	0.17	-0.05	0.31	0.55	-0.50	-0.22	-0.02	-0.39
Nd	0.71	0.89	0.48	0.58	0.22	0.17	-0.06	0.32	0.57	-0.52	-0.22	.003	-0.41
Sm	0.71	0.90	0.49	0.58	0.22	0.18	-0.08	0.36	0.58	-0.53	-0.23	-.001	-0.42
Eu	0.63	0.86	0.45	0.49	0.23	0.20	-0.05	0.40	0.57	-0.51	-0.21	-0.03	-0.41
Gd	0.71	0.89	0.48	0.58	0.22	0.19	-0.07	0.36	0.57	-0.51	-0.22	0.01	-0.40
Tb	0.72	0.87	0.51	0.61	0.22	0.25	-0.06	0.45	0.60	-0.46	-0.19	-0.07	-0.37
Dy	0.71	0.87	0.52	0.59	0.24	0.26	-0.09	0.46	0.62	-0.48	-0.17	-0.04	-0.39
Er	0.71	0.85	0.54	0.60	0.26	0.35	-0.09	0.54	0.65	-0.42	-0.13	-0.10	-0.36
Tm	0.66	0.84	0.57	0.56	0.29	0.37	-0.12	0.58	0.67	-0.44	-0.15	-0.15	-0.38
Yb	0.71	0.82	0.59	0.63	0.29	0.40	-0.11	0.60	0.70	-0.40	-0.11	-0.18	-0.35
Lu	0.73	0.81	0.6	0.65	0.29	0.40	-0.11	0.59	0.71	-0.41	-0.12	-0.18	-0.37
∑ REE	0.71	0.86	0.47	0.60	0.21	0.19	-0.04	0.33	0.55	-0.48	-.20	-0.02	-0.38

As it could be seen in the above table, the good correlations of 0.71 and 0.86 were reported between the REEs with U and K. This value between REEs and CPS is also acceptable (0.6). Moreover, there is a strong correlation between uranium and CPS. Therefore, it could be thought that U is the main source of radioactivity.

Actually, the correlation coefficient of REEs with U and Th is greater than CPS, and this amount is more for CPS than K.

Apart from the cases mentioned above, no significant correlation coefficient can be observed for the other elements.

As it can be seen in the above diagrams, the correlation for REEs with Th and U is more than REEs and CPS, and the correlation between REEs and potassium is very low (similar to the results in Table 6).

The results of statistical studies show that Baghak anomaly due to involving a significant amount of U, Ce, and La, and a high concentration of REEs could be considered as one of the important mines. For this reason, in the next section, the normalized REE distribution patterns (based on the chondrite and primitive mantle) were studied and investigated in the Baghak mine. Finally, in order to confirm the skarn mineralization type of the Baghak mine, its chondrite-normalized REEs distribution pattern was compared with the REE distribution patterns related to several different types of iron deposits (skarn, Banded Iron Formation (BIF), hydrothermal, and Kiruna).

4.3. Spider diagram analysis

The spider diagrams were firstly drawn, and then were analyzed. In order to achieve this goal and to reduce the number of lines for 151 samples, in the first step, 151 samples were divided into 5 groups of 25 samples each and one group of 26 samples, and then the average of each group was considered as a sample. In fact, by doing so, we had six samples that were representatives of 151 samples from different points of the boreholes, and the average of each group was considered as a new sample. Then in the next step, the spider diagrams of chondrite-normalized REEs were provided for the above-mentioned groups (average of the six groups) (Figure 11 A) and for one sample that was the average value of 151 samples (Figure 11 B).

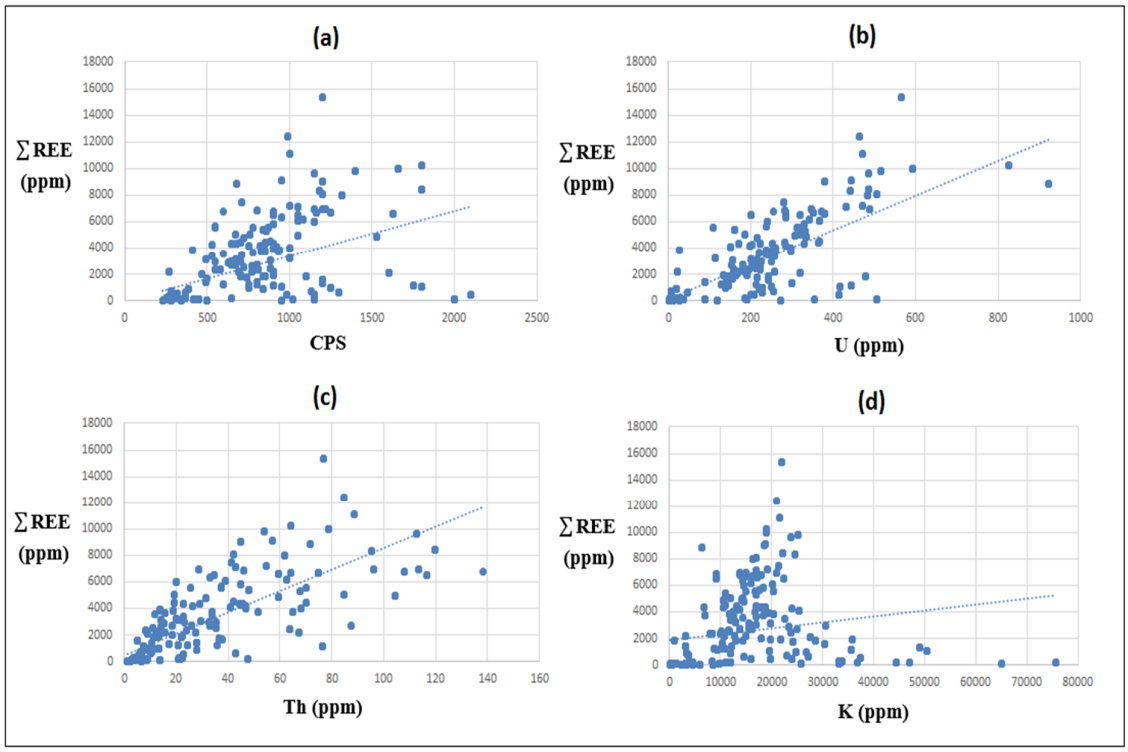

Figure 11. Dispersion diagrams of REEs and CPS (a), REEs and U (b), REEs and Th (c) REEs and K (d).

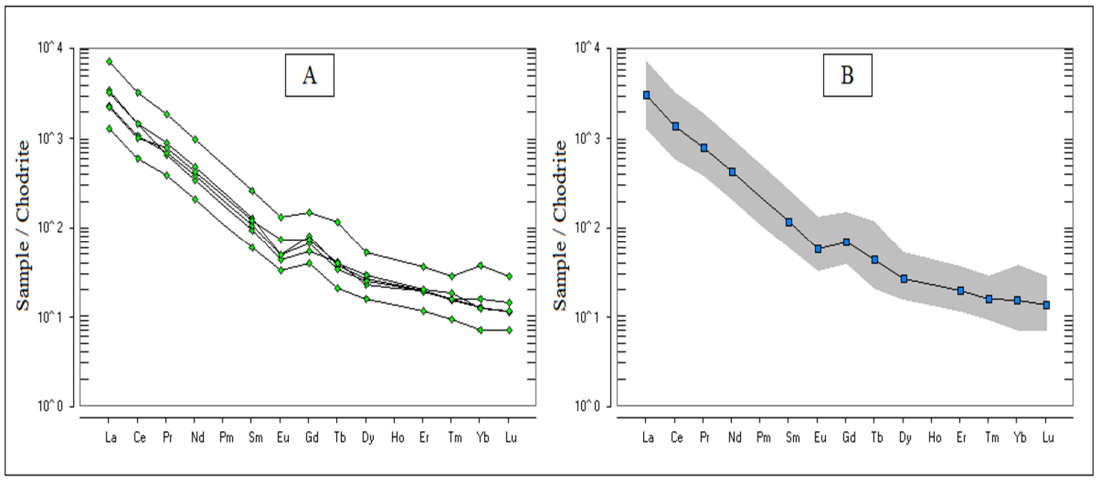

Figure 11. Chondrite-normalized REE patterns for A: representative samples relative to six groups from the total samples, B: one sample that is the average value of 151 samples (in the halo of part A) (values from [24]).

Similar to the above diagrams, another diagram was also drawn for the mineralization samples (in terms of uranium). In this way, 125 mineralized samples were divided into 5 groups of 25 samples each, and the average of each group was considered as a new sample. Finally, the chondrite-normalized pattern of 5 samples (representative samples for the 5 above-mentioned groups) along with a sample that was the average of all mineralized samples was prepared and shown in Figure 12.

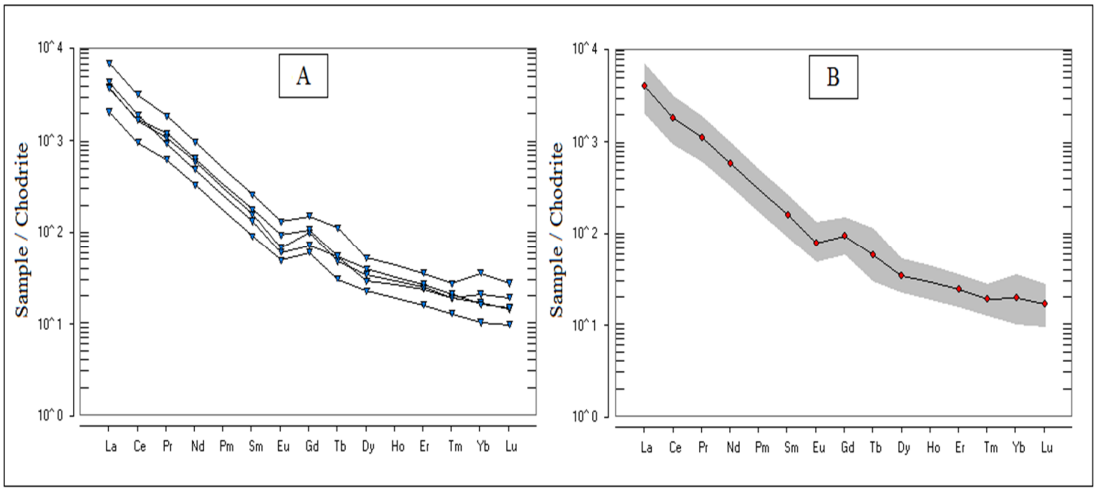

Figure 12. Chondrite-normalized REE patterns for A: representative samples relative to five groups from mineralization samples, B: one sample that is the average value of mineralization samples (in the halo of part A) (values from [24]).

The primitive mantle normalized trace and REE pattern for the above-mentioned groups (average of the six groups) and for one sample that is the average value of 151 samples are provided and illustrated in Figure 13.

5. Discussion

The microscopic studies show that:

- REEs, especially Ce, are present in the samples (lanthanum and neodymium are also observed at a section).
- REEs are accumulated as a solid solution in the allanite minerals.
- Allanite minerals can be seen with a high amount in the studied samples, and the high values of REEs in elemental analyses are also related to this mineral.
- REEs cannot be observed in the network of other minerals, particularly the Fe-bearing minerals (magnetite).
- Uranium is formed as allanite-independent minerals or, in other words, out of silicate network of allanite. Actually, uranium has been

mostly trapped as inclusions in empty spaces of allanite and also Fe-bearing minerals.

According to the values reported from the elemental analysis, prospecting of REEs in this anomaly is dependent on the prospecting method of radiation measurement presented in this work. It was revealed that the correlation coefficient between REEs and radioactivity (CPS) was 0.6, and also there was an acceptable and high correlation between REEs with the uranium and thorium concentrations (respectively, 0.71 and 0.86).

The major origin of radioactivity in the studied area is uranium, and radioactivity is more affected by this element because a) the correlation between CPS and uranium (0.91) is much greater than that of thorium and potassium (respectively, 0.52 and 0.46), b) the mineralization nature is poor in terms of thorium, and its correlation with REEs is related to the little amount of thorium (according to the amount of 26 ppm reported in Table 5),c) potassium involves less share of radioactivity (its correlation with CPS is 0.46), and it could be said that a decrease in the correlation coefficients between REEs and radioactivity (CPS) compared to the correlation coefficients between REEs and the two elements of U and Th is caused by the K effect on the measured radioactivity by the spectrometer.

Thus in the statistical studies of the results of geochemical analysis of the samples taken from the Baghak anomaly, it was observed that in addition to the relation of REEs and radioactivity, particularly in the case of U and Th in Central Iran mineralizations, there is a similar relation in skarn mineralization. These elements show a thermodynamic behavior similar to U and Th, and they are solved and moved as different complexes mostly as $REEF_3$ and $REECl_3$ under deep reduction conditions and a low oxygen fugacity, and they are placed as $REEO_2$ or REE_2O_3 under

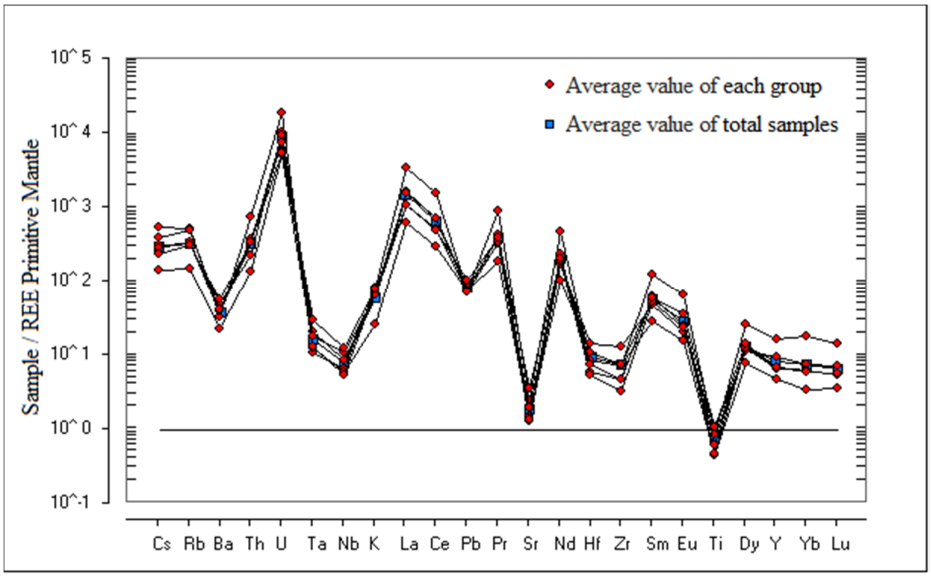

Figure 13. Primitive mantle normalized trace and REE pattern for the 151 samples under investigation (values from [25]).

the oxidation condition in crystal network of minerals located at the fluid crystallization end series.

Comparison of Figures. 10 and 11 also shows the relationship between REEs and the uranium element since the halo of the distribution pattern of normalized REEs related to the mineralization samples (Figure 11) has significantly decreased compared to the halo of the whole samples (151 samples) (Figure 10). That means that the decrease in the uranium grade decreases the amount of REEs as well so that this decrease is clearly visible in the normalized REE distribution pattern (Figures. 10 and 11).

Another point that can be extracted from the above diagrams (Chondrite-normalized REEs) is the moderately strong LREE enrichment relative to the almost descending trend close to flat of HREE, which confirms the formation of magma in the subduction zone [10, 26-28].

In fact, since HREE tends to remain in the remaining melt in magma (during the process of subtraction of magma), it shows a depletion in the chondrite-normalized REE diagrams. Furthermore,

the presence of high volumes of OH rich fluid and alterations resulting from it could also be the reason for the decrease of LREE/HREE in the spider diagrams. Moreover, it is possible that the early magma is inherently poor in terms of HREE.

Barati and Gholipour believed that the reason for LREE enrichment relative to HREE in the Zafarabad Magnetite samples (Kurdistan, Iran) was the entry of LREE in the magnetite network since magnetite could have up to 67.6 percentage weight of Ca [29]. They have stated that if a large cation such as Ca could enter the network of magnetite, the possibility of entering the REE ions, which are similar to Ca in terms of ionic radius is also present in the magnetite network [29].

They also acknowledged that since LREE had an ionic radius closer to Ca, it was possible to replace it in the magnetite network (instead of Ca), and it was the reason for its enrichment relative to HREE [29].

The results of SEM studies at the Baghak mine reject this possibility about the Baghak mine magnetite. The results of SEM studies at the Baghak mine indicate that REEs are not present in the network of magnetite and Fe-bearing minerals (in none of the samples). Moreover, it can be seen that the observed REEs (serum, lanthanum, and neodymium) in the SEM results, especially the element of cerium, are solely present in the network of allanite minerals.

As mentioned earlier, allanite is from the epidote group, and its general formula is $Ca_2(Al,Fe)_3(OH)(SiO_4)_3$ [19]. Fe, Ce, and Al enter the solid solution of the mentioned composition under particular conditions, and allanite is generated by the formula of $(Ca,Fe^{2+})_2(Al,Ce,Fe^{3+})_2(OH)(SiO_4)_3$ [20-21].

Thus according to the above explanations, it can be admitted that the REE ions that are similar to Ca ions (in terms of the ionic radius) enter the allanite network as solid solutions, and since LREE has an ionic radius closer to Ca, it replaces Ca in the allanite network.

The above hypothesis could be considered as a valid event because the SEM results also indicate the replacement of REE, especially cerium, instead of Ca in the network of allanites.

In the mentioned diagrams (Chondrite-normalized REEs), depletion of Eu is also observed in comparison with the other elements, which may be related to the crystallization of the plagioclase from mineralization magmatism [2] or it is possible that magma is poor in terms of Eu. Moreover, the relatively low severity of this anomaly could also be due to the sub-division of the Earth's crust.

In the diagram in Figure 12, the LREE enrichment such as Ce, La, Pr, and Nd, and the radioactive element U are clearly evident. It could also be due to the similarities that have been mentioned in the previous section (between REEs and the radioactive elements, especially U). It can also be seen an enrichment in large ion lithophile (LILE; Cs, Rb, Ba, K) and in incompatible elements that behave similar to LILE (U, Th) and a relative depletion in high field strength elements (HFSE; Nb, Y, Ti, Ta, Zr) and HREE (Yb, Lu) (Ti depletion is relative to the primitive mantle). These features are typical of the subduction related magmas in the calcalkaline volcanic arcs of continental active margins [26, 30-31]. Their low Sr, Nb, Ta, and Ti contents are thought to be due to the presence of Ti (Nb) minerals (rutile and ilmenite) and plagioclase or Fe–Ti oxides in the residue left in the source area of the parental magmas [32-34].

Finally, in order to investigate the type of iron mineralization in the Baghak mine and based on the spider diagrams that were depicted in the previous section, the REE distribution pattern was compared with the REE distribution pattern related to several different types of iron deposits (skarn, Banded Iron Formation (BIF), hydrothermal, and Kiruna) (Figure 13).

In Figure 13 (part A), the REE pattern for the samples of magnetite of hydrothermal iron deposits is shown, in which is seen a highly enrichment in LREE compared to HREE and almost from La to Lu with a steep slope is dwindling in the descending order. The positive Eu anomaly is also visible in this diagram. In fact, these two features are the typical characteristics of the hydrothermal deposits.

Part B of Figure 13 is also related to the BIF deposits with positive Eu anomalies, and severe negative anomalies of Ce are considered as their main characteristics. The addition of hot and Eu-rich hydrothermal fluids to oceans is considered as a reason for the positive Eu anomaly in this type of deposit [39]. Moreover, severe negative Ce anomalies are one of the most characteristic features of submarine hydrothermal iron deposits [40]. In fact, the presence of positive anomalies of Eu and negative Ce anomaly together in sedimentary iron deposits indicate that the ore is deposited in the form of chemical sedimentation and in the presence of submarine hydrothermal fluids.

Figure 13 C shows the REE distribution pattern in the magnetite iron deposits of Kiruna type. Magnetite ores of different types of

palaeoproterozoic in the north of Sweden are relatively poor in REEs, and there is a slight differentiation between LREE and HREE in magnetite of these deposits.

Finally, part D of Figure 13 shows the REE distribution pattern for magnetite ore of iron skarn deposits in the Misi regions, Finland. LREE enrichment relative to the flattening trend of HREE, and also the mild anomaly of Eu is the most important feature of this diagram.

Comparison of the two Figures 10 and 13 shows that differences such as positive Eu anomalies in cases A and B, equal slope of La to Lu in the case of A, severe negative anomalies of Ce in the case of B, and negative anomalies of Gd in part C, separated REEs patterns in the Baghak mine from the proposed patterns for hydrothermal, BIF and Kiruna deposits.

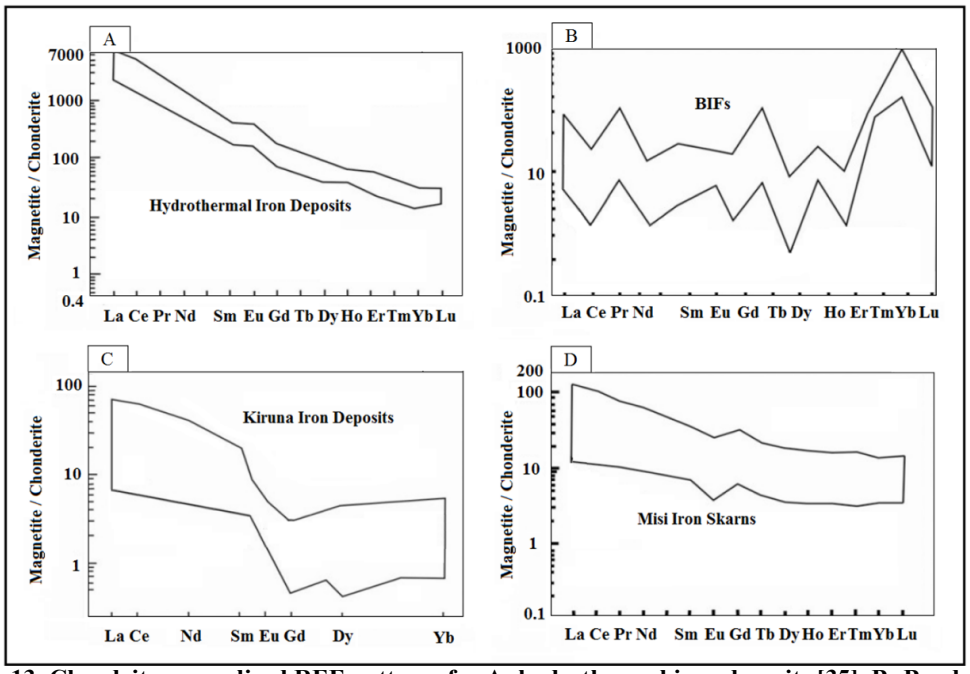

Figure 13. Chondrite-normalized REE patterns for A: hydrothermal iron deposits [35], B: Banded iron formation [36], C: Kiruna iron deposits [37], and D: Misi iron skarns [38].

There are similarities including the LREE enrichment relative to the flattening trend of the HREE as well as the negative Eu anomaly between the REE distribution pattern in the Baghak mine and in the samples of iron skarn deposits in the Misi areas of Finland so that according to the presented distribution pattern of REEs for these two ore deposits, a nearly apparent downward trend in the LREE relative to a downward trend and near-flat slope for HREE is considered as a criterion for distinguishing between these two elemental groups (LREE enrichment compared to HREE).

6. Conclusions

According to the Sangan geology, and especially Baghak anomaly, the carbonate rocks aged Cretaceous are mostly dolomite-limestone. Syenogranite to monzonite intrusive bodies and also syenite by the porphyry texture caused skarn and Fe mineralization (magnetite).

- It was revealed in the preliminary studies that REEs such as La, Nd, and especially Ce aggregated as a solid solution in allanite, which was significantly observed in the sections. Then based on the mineralogical studies, observing LREE in the allanite network using SEM, and also according to the normalized REEs pattern, it was concluded about the mineralization of REEs and radioactive elements that REEs were formed as a solid solution in silicate minerals, particularly allanite, which was from the epidote group in a high temperature phase and probably at the same time with skarn. In other words, REEs, especially Ce, have substituted Ca due to a similar ionic radius in the allanite network. This also happened for Th and REEs but due to a low concentration of Th in the mineralizing fluids, there is no sign of high enrichment. Therefore, little amount of Th along with REEs was placed in the silicate network of allanite and explicit relation of radioactive elements and REEs (in

addition to such relation in Central Iran) observed in the Baghak anomaly mineralization.

- After that, it was seen that a chondrite-normalized REEs pattern showed enrichment of LREE and a positive pattern close to flat HREE due to the entry of LREE ions into the allanite network. Moreover, the negative Eu anomaly in the normalized REE pattern relative to the total samples indicated that the source magma was plagioclase-bearing.
- The results obtained also show that the primitive mantle normalized rare earth and trace elements pattern is enriched with LREE (La, Ce, Pr, Nd), in large ion lithophile (LILE, Cs, Rb, Ba, K), in radioactive elements that behave similar to LILE (Th, U), and are strongly depleted in high field strength elements (HFSE, Y, Zr, Ta, Nb, Ti) and HREE (Yb, Lu) compared to the primitive mantle. These features are typical of the subduction related magma.
- Finally, the results of comparing REE distribution pattern in Baghak with several different types of ores confirm skarn mineralization type in Baghak mine, which is very similar to the Misi region in Finland.

Acknowledgment

We would like to thank the Sangan Iron Ore Complex for the access to the mine data.

References

[1]. Ghannadpour, S.S. (2014). Geochemical and metallurgical studies of rare earth elements and evaluating their potential in Bafq-Robat Posht-e Badam belt. Atomic Energy Organization of Iran (Under Supervision of I.R. IRAN National Elites Foundation). Tehran, Report, 162 p. (in Persian with English abstract).

[2]. Malekzadeh Shafaroudi, A., Karimpour, M. H. and Golmohammadi, A. (2013). Zircon U-Pb geochronology and petrology of intrusive rocks in the C-North and Baghak districts, Sangan iron mine, NE Iran. Journal of Asian Earth Sciences, vol. 64, 256-271.

[3]. Boomeri, M. (1998). Petrography and geochemistry of the Sangan iron skarn deposit and related igneous rocks, NE Iran. PhD thesis, Akita University, Japan, 226 p.

[4]. Boomeri, M. (2006). Rare earth elements (REEs) in garnet of Sangan iron ore deposit. Geological Society of Iran, Tehran Tarbiat Moallem University, Tehran, Iran (in Persian).

[5]. Mazhari, N., Malekzadeh Shafaroudi, A. and Ghaderi, M. (2017). Detecting and mapping different types of iron mineralization in Sangan mining region, NE Iran, using satellite image and airborne geophysical data. Geoscience Journal, vol. 21, 137-148.

[6]. Mazhari, N., Malekzadeh Shafaroudi, A. and Ghaderi, M. (2015). Geology, mineralogy, and geochemistry of Ferezneh ferromanganese anomaly, east of Sangan mines complex, NE Iran. Journal of Economic Geology, vol. 7(1), 23-37.

[7]. Mazhari, N., Malekzadeh Shafaroudi, A. and Ghaderi, M. (2016). Geochemistry of intrusive rocks, petrology of skarn, and mineralogy and chemistry of orebodies in Senjedak-I area, east of Sangan mine, Khaf, NE Iran. Scientific Quaterly Journal, GEOSCIENCES, vol. 25 (100): 235-246 (in Persian with English abstract).

[8]. Golmohammadi, A., Mazaheri, S. A., Karimpour, M.H. and Malekzadeh Shafaroudi, A. (2014). Zircon U-Pb dating and geochemistry of Sarkhar and Bermani granitic rocks, East of Sangan iron mine, Khaf. Journal of Petrology, vol. 5 (17): 83-102 (in Persian with English abstract).

[9]. Golmohammadi, A., Karimpour, M.H., Malekzadeh Shafaroudi, A. and Mazaheri, S.A. (2013). Petrology and U-Pb zircon dating of intrusive rocks from A, C-south, and Dardvay districts, Sangan iron stone mine, Khaf. Journal of Economic Geology, vol. 2 (5): 157-174 (in Persian with English abstract).

[10]. Golmohammadi, A., Karimpour, M.H., Malekzadeh Shafaroudi, A. and Mazaheri, S.A. (2015). Alteration-mineralization and radiometric ages of the source pluton at the Sangan iron skarn deposit, NE Iran. Ore Geology Reviews, vol. 65 (2): 545-563.

[11] Gholipour, B., Kananian, A. and Niromand, S. (2019). Application of geochemical data in recognizing conditions of rare earth element concentrations in southern C mine anomaly of Sangan iron skarn, Khorasan Razavi. Journal of Advanced Applied Geology, vol. 9 (1(31)): 38-49.

[12]. Sepidbar, F., Mirnejad, H., Li, J.W., Wei, C., George, L.L. and Burlinson, K. (2017). Mineral geochemistry of the Sangan skarn deposit, NE Iran: Implication for the evolution of hydrothermal fluid. Chemie der Erde, vol. 77, 399–419.

[13]. Deymar, S., Behzadi, M. and Yazdi, M. (2019). Relation of alkali-metasomatism and Ti-REE-U (Th) mineralization in the Saghand mining district, Central Iran. Journal of Economic Geology, vol. 10 (2): 471-296.

[14]. Vural, A. (2020). Investigation of the relationship between rare earth elements, trace elements, and major oxides in soil geochemistry. Environmental Monitoring and Assessment, vol. 192, 124.

[15]. Cunha, C.S.M., Escobar, M.E.O., da Silva, Y.J.A.B., do Nascimento, C.W.A. (2018). Spatial variability and geochemistry of rare earth elements in soils from the largest uranium–phosphate

deposit. Environmental Geochemistry and Health, vol. 40, 1629–1643.

[16]. Ling, M., Yang, X., Sun, W., Miao, J. and Liu, C. (2006). REE/trace element characteristics of sandstone-type uranium deposits in the Ordos Basin. Chinese Journal of Geochemistry, vol. 25 (4): 354-364.

[17]. Karimpour, M. H. and Malekzadeh Shafaroudi, A. (2007). Skarn Geochemistry-Mineralogy and Petrology of Source Rock Sangan Iron Mine, Khorasan Razavi, Iran. Scientific Quaterly Journal, GEOSCIENCES, vol. 17(65), 108-125 (in Persian with English abstract).

[18]. Iran Eastern Iron Ore Co. (2011). Modelling, types, classification, and calculation of iron deposit in Baghak mine. Report, Sangan Iron Ore Complex.

[19]. Rabadjieva, D., Tepavitcharova, S., Todorov, T., Dassenakis, M., Paraskevopoulou, V. and Petrov, M. (2009). Chemical speciation in mining affected waters: the case study of Asarel-Medet mine. Environmental Monitoring and Assessment, vol. 159, 353–366.

[20]. Ercit, T.S. (2002.) The mess that is 'allanite'. The Canadian Mineralogist, vol. 40, 1411-1419.

[21]. Gregory, C.J., Rubatto, D., Allen, C., Williams, I.S. and Hermann, J. (2007). Ireland TR. Allanite micro-geochronology: a SHRIMP and LA-ICP-MS study. Chemical Geology, vol. 245, 162–182.

[22]. Guastoni, A., Nestolal, F. and Schiazza, M. (2017). Post-magmatic solid solutions of $CaCeAl_2(Fe^{3+}_{2/3}\square_{1/3})[Si_2O_7]$ $[SiO_4]O(OH)$, allanite-(Ce) and REE-bearing epidote in miarolitic pegmatites of Permian Baveno granite (Verbania, central-southern alps, Italy). Mineralogy and Petrology, vol. 111, 315–323.

[23]. Hezarkhani, A. and Ghannadpour, S.S. (2015). Exploration Information Analysis, first ed: Amirkabir University of Technology (Tehran Polytechnic) press, Tehran (in Persian with English abstract).

[24]. Boynton, W.V. (1983). Cosmo-chemistry of the rare earth elements: meteorite studies", in: P. Henderson (editor), Rare earth element geochemistry, Elsevier, Amsterdam, chapter 3, 63-114.

[25]. McDonough, W.F. and Sun, S.S. (1995). The composition of the Earth. Chemical Geology 120: 223-254.

[26]. Gill JB. (1981). Orogenic Andesites and Plate Tectonics. Springer-Verlag, Berlin, 390 p.

[27]. Rollinson, H. (1993). Using geochemical data, Evaluation, Presentation, Interpretation, Harlow. Longman Scientific & Technical, Harlow, UK, 352 p.

[28]. Wilson, M. (2007). Igneous Petrogenesis: A Global Tectonic Approach. Springer (originally published by Chapman and Hall), Netherlands, 466 p.

[29]. Barati, M. and Gholirpour, M. (2014). Mineralogy, geochemistry, and origin of Zafarabad iron ore deposit in Kurdistan using rare earth element data of magnetite mineral. Journal of Economic Geology, vol. 5 (2): 235-254 (in Persian).

[30]. Pearce, J.A. (1983). Role of the sub-continental lithosphere in magma genesis at active continental margins. in: Hawkesworth, C.J., Norry, M.J. (Eds.), Continental Basalts and Mantle Xenoliths, Shiva, Nantwich, 230–249.

[31]. Walker, J.A., Patino, L.C., Carr, M.J. and Feigenson, M.D. (2001). Slab control over HFSE depletions in central Nicaragua. Earth and Planetary Science Letters, vol. 192, 533–543.

[32]. Reagan, M.K. and Gill, J.B. (1989). Co-existing calc-alkaline and high niobium basalts from Turrialba volcano, Costa Rica: implication for residual titanates in arc magma source. Journal of Geophysical Research, vol. 94, 4619–4633.

[33]. Pearce, J.A. and Parkinson, I.J. (1993). Trace element models for mantle melting: application to volcanic arc petrogenesis. in: Prichard, H.M., Albaster, T., Harris, N.B.W., Neary, C.R. (Eds.), Magmatic Processes in Plate Tectonics. Geological Society of London Special Publication, vol. 76, 373–403.

[34]. Martin, H. (1999). The adakitic magmas: modern analogues of Archaean granitoids. Lithos, vol. 46, 411–429.

[35]. Tallarico, F.H.B., Figueiredo, B.R., Groves, D.I., Kositcin, N., McNaughton, N.H., Fletcher, I.R. and Rego, J.L. (2005). Geology and SHRIMP U-Pb geochronology of the Igarape Bahia deposit, Carajas copper-gold belt, Brazil: An Archean (2.57 Ga) example of iron-oxide Cu-Au-(U-REE) mineralization. Economic Geology, vol. 100, 7–28.

[36]. Oksuz, N. and Ko, S. (2009). Examination of Sarikaya (Yozgat-Turkey) iron mineralization with rare earth element (REE) method. Journal of Rare Earths, vol. 28 (1): 143–149.

[37]. Frietsch, R. and Pendahl, J.A. (1995). Rare earth elements in apatite and magnetite in kiruna-type iron ores and some other Iron types. Ore Geology Reviews, vol. 9, 489-510.

[38]. Niiranen, T., Manttari, I., Poutiainen, M., Oliver, N. and Miller, J.A. (2005). Genesis of Palaeoproterozoic iron skarns in the Misi region, northen Finland. Mineralium Deposita, vol. 40, 192–217.

[39]. Barret, T.J., Fralick, P.W. and Jarvis, I. (1988). Rare earth element geochemistry of some Archean iron formations North of Lake Superior, Ontario. Canadian Journal of Earth Science, vol. 25 (4): 570–580.

[40]. Fryer, B.J. (1977). Rare earth evidence in iron formations for changing Precambrian oxidation states. Geochemica et Cosmochimica Acta, vol. 41, 361–367.

بررسی همبستگی ژئوشیمیایی بین عناصر پرتوزا و نادر خاکی؛ مطالعه موردی: معدن باغک، شمال شرق ایران

سید سعید قنادپور* و اردشیر هزارخانی

دانشکده مهندسی معدن و متالوژی، دانشگاه صنعتی امیرکبیر، تهران، ایران

ارسال ۲۰۲۱/۰۵/۰۴، پذیرش ۲۰۲۱/۰۶/۰۳

* نویسنده مسئول مکاتبات: s.ghannadpour@aut.ac.ir

چکیده:

در برخی از پروژه‌های پی‌جویی اورانیوم در ایران، به ویژه ایران مرکزی، ارتباط و غنی سازی عناصر نادر خاکی (REE) به عنوان یک ویژگی معمول شناخته شده است. در بعضی مواقع همراهی عناصر نادر خاکی با چشم‌انداز اقتصادی بالا، باعث شده است ارتباط عناصر نادر خاکی و عناصر پرتوزا در دیگر کانی سازی‌ها نیز مورد توجه قرار گیرد و در صورت وجود چنین رابطه‌ای، اندازه‌گیری پرتوزایی در اکتشاف عناصر نادر خاکی در نظر گرفته شود. در این مطالعه، بر مبنای اندازه‌گیری مقدار پرتوزایی، به نمونه‌برداری از آنومالی باغک در معدن سنگان پرداخته شده است (به عنوان یک الگوی نمونه‌برداری بهینه). در واقع هدف از این کار، بررسی چنین رابطه‌ای در یک معدن اسکارنی به عنوان یک مطالعه موردی متفاوت از کانی‌سازی‌های ایران مرکزی است که در صورت وجود آن، این روش را می‌توان به عنوان یک الگوی اکتشافی جدید و بهینه در مورد عناصر نادر خاکی در نظر گرفت. بدین منظور از مطالعات کانی‌شناسی (بر اساس مشاهدات میکروسکوپی نوری و الکترونی)، بررسی‌های آماری و ژئوشیمیایی بهره گرفته شده است. نتایج بدست آمده از مطالعات آماری نشان می‌دهد که آنومالی باغک به واسطه وجود مقدار قابل توجهی از عناصر اورانیوم، سریم و لانتانیوم، می‌تواند به عنوان یکی از معادن مهم در نظر گرفته شود. بررسی‌های ژئوشیمیایی و نمودار عنکبوتی نشان‌دهنده ماگمای مرتبط با مناطق فرورانش در قوس‌های آتشفشانی کالک‌آلکالن حاشیه فعال قاره‌ای است. نتایج حاصله از الگوی هنجار شده به کندریت‌ها نیز نشان دهنده غنی‌شدگی از LREE نسبت به روند نزولی و نزدیک به مسطحی از HREE می‌باشد که دلیل آن ورود یون‌های LREE به داخل شبکه آلانیت‌ها ست. نتایج مطالعات کانی شناسی نیز تجمع عناصر نادر خاکی (به‌ویژه سریم) را در شبکه کانی‌های آلانیت تایید می‌کنند. از تجربه و تحلیل‌های آماری، ژئوشیمیایی و کانی‌شناسی می‌توان مشاهده کرد که علاوه بر وجود چنین رابطه‌ای در برخی کانی‌سازی‌های ایران مرکزی، در آنومالی باغک (به عنوان یک کانی سازی آهن-اسکارن) نیز همبستگی قابل قبولی بین آنها وجود دارد. در نهایت می‌توان اذعان داشت که معرفی این ایده و الگوی نمونه‌برداری جهت اکتشاف عناصر نادر خاکی می‌تواند دیدگاه مناسبی را در اختیار تصمیم‌گیران این صنعت قرار دهد.

کلمات کلیدی: اندازه‌گیری پرتوزایی، رادیواکتیویته، عناصر نادر خاکی، باغک، معدن آهن سنگان.